Long-Wavelength Helimagnetic Order and Skyrmion Lattice Phase in Cu_2OSeO_3

T. Adams,[1] A. Chacon,[1,2] M. Wagner,[1] A. Bauer,[1] G. Brandl,[1,2] B. Pedersen,[2] H. Berger,[3] P. Lemmens,[4] and C. Pfleiderer[1,*]

[1]*Technische Universität München, Physik-Department E21, D-85748 Garching, Germany*
[2]*Forschungsneutronenquelle Heinz Maier Leibnitz (FRM II), Lichtenbergstr. 1, 85748 Garching, Germany*
[3]*Ecole Polytechnique Federale Lausanne, CH-1015 Lausanne, Switzerland*
[4]*Institute for Condensed Matter Physics, TU Braunschweig, D-38106 Braunschweig, Germany*
(Received 21 February 2012; revised manuscript received 9 April 2012; published 8 June 2012)

We report a long-wavelength helimagnetic superstructure in bulk samples of the ferrimagnetic insulator Cu_2OSeO_3. The magnetic phase diagram associated with the helimagnetic modulation inferred from small-angle neutron scattering and magnetization measurements includes a skyrmion lattice phase and is strongly reminiscent of MnSi, FeGe, and $Fe_{1-x}Co_xSi$, i.e., binary isostructural siblings of Cu_2OSeO_3 that order helimagnetically. The temperature dependence of the specific heat of Cu_2OSeO_3 is characteristic of nearly critical spin fluctuations at the helimagnetic transition. This provides putative evidence for effective spin currents as the origin of enhancements of the magnetodielectric response instead of atomic displacements considered so far.

DOI: 10.1103/PhysRevLett.108.237204 PACS numbers: 75.25.−j, 75.50.Gg, 75.85.+t

Major efforts have been made recently to unravel the nature of the magnetoelectric coupling in multiferroic materials [1–4]. Amongst a wide range of theoretical scenarios, two mechanisms are considered most prominent. First, a coupling mediated by effective spin currents in spin spiral magnets and, second, an exchange striction mechanism in which the magnetoelastic coupling proceeds via atomic displacements. An important property believed to provide unambiguous evidence of the latter mechanism is an enhancement of the magnetodielectric response (MDR), describing changes in the dielectric polarization in the presence of magnetic fields or magnetic order. However, the discovery of an enhanced MDR near the magnetic transition of the insulator Cu_2OSeO_3 appears to question this view [5]. Detailed studies of the crystal structure and lattice dynamics strongly suggest the absence of spontaneous lattice strains [5–8]. Being a lone pair containing piezoelectric ferrimagnet, this was taken as evidence of a new magnetoelectric coupling mechanism. Yet, enhancements of the MDR without lattice strains are not specific to multiferroics and represent a more general scientific challenge. For instance, the spin ice system $Dy_2Ti_2O_7$ displays an enhanced MDR but is neither magnetically ordered nor multiferroic [9].

Cu_2OSeO_3 is ideally suited to study enhancements of the MDR without lattice strains. It crystallizes in the noncentrosymmetric space group $P2_13$ [10], which structurally allows ferroelectricity. The unit cell is composed of three building blocks [11]. The first and the second building block are given by a square pyramidal and a trigonal bipyramidal CuO_5 unit in a three to one ratio, respectively. The third building block is a lone pair containing a tetrahedral SeO_3. Magnetization measurements and powder neutron diffraction have established ferrimagnetic order of the Cu^{2+} moments below $T_c = 58.8$ K, where three ferromagnetically aligned Cu moments pair up antiferromagnetically with a fourth Cu moment [5,12]. The exchange coupling is given by $J_{FM} = -50$ K and $J_{AFM} = 68$ K for the ferromagnetic and antiferromagnetic exchange, respectively, consistent with the Kanamori—Goodenough rules [13].

However, a description as a ferrimagnet seems incomplete. First, well below T_c, the magnetization increases almost linearly with increasing field before saturating above ~120 mT without evidence for a spontaneous uniform magnetic moment at $B = 0$ [5,14,15]. If the behavior for $B \lesssim 120$ mT would be due to magnetic domains, the slope and the onset of saturation would sensitively reflect demagnetizing fields and depend on sample shape which is not observed. Second, small changes of slope in the initial increase of $M(B)$ suggest that the magnetic state is more complex [14]. Third, the ferrimagnetic order is incompatible with the $P2_13$ space group, and a symmetry lowering transition is expected which is not observed [5,8,13,14]. Finally, a detailed magnetic phase diagram of bulk samples was recently determined in magnetization and electric polarization measurements along the $\langle 111 \rangle$ axes only [16,17]. Using Lorentz force microscopy in thin Cu_2OSeO_3 samples, helimagnetic order and a skyrmion lattice phase were observed, but the phase diagram had completely different phase boundaries. Moreover, for the thin samples, the helical order was found to propagate along $\langle 110 \rangle$, which is not favored by the $P2_13$ space group in bulk samples. This questions the reported magnetoelectric coupling [17,18].

In this Letter we report a helimagnetic superstructure in *bulk samples* of Cu_2OSeO_3, which resolves all of the questions listed above and suggests strongly that the

enhanced MDR arises from spin currents due to nearly critical helimagnetic spin fluctuations. The helimagnetic order in Cu_2OSeO_3 relates thereby to binary transition metal compounds such as MnSi and FeGe, which share the space group $P2_13$ with Cu_2OSeO_3, supporting a hierarchy of three energy scales in their B20 crystal structure [19]. These are ferromagnetic exchange and Dzyaloshinsky—Moriya interactions on the strongest and second strongest scale, respectively, generating a long-wavelength helimagnetic modulation. The propagation direction of the helix is finally the result of very weak magnetic anisotropies on the weakest scale. Most spectacular, a skyrmion lattice phase was recently discovered in binary $P2_13$ transition metal compounds [20–23], giving rise to an emergent electrodynamics [24,25].

Small-angle neutron scattering (SANS), magnetization, and specific heat measurements were carried out on a single crystal, where we refer to the Supplemental Material [26] for details on the experimental method. Shown in Fig. 1(a) is $M(T)$ in the vicinity of T_c. Well above T_c, a strong Curie-Weiss dependence with $\mu_{\rm CW} \approx 1.5\mu_{\rm B}/{\rm Cu}$ in perfect agreement with the literature. With increasing field, the magnetization increases. In the vicinity of T_c, faint maxima develop as illustrated in Fig. 1(b), where M/B is shown for clarity. These features are analogous to MnSi [27], where they arise from the skyrmion lattice phase. The temperature dependence is consistent with the field dependence shown in Figs. 1(c) through 1(k) for field along ⟨100⟩, ⟨110⟩, and ⟨111⟩. With decreasing temperature, $M(B)$ increases before reaching a saturated moment $m_s = 0.48\mu_{\rm B}/{\rm Cu}$ at large fields. The susceptibility $\mu_0 dM/dB$ reveals a distinct minimum in a small T interval as illustrated in Figs. 1(e), 1(h), and 1(k). We thereby define transition fields B_{c1}, B_{A1}, B_{A2}, and B_{c2} (Fig. 1) as in the binary $P2_13$ compounds [28].

From the magnetization, we infer the phase diagrams shown in Fig. 2. The SANS data described below identify the following phases: (i) for $B < B_{c1}$, helimagnetic order denoted h, (ii) for $B_{c1} < B < B_{c2}$, conical order denoted c, (iii) for $B > B_{c2}$, field-polarized ferrimagnetic order, and finally (iv) a skyrmion lattice in the regime denoted A, just below T_c. We note that differences of B_{c2} reflect demagnetizing fields, which cannot be corrected accurately for the shape of our sample. Likewise, the field range of the skyrmion lattice phase varies weakly with field direction [Figs. 2(b)–2(d)]. However, the temperature range is clearly largest for ⟨111⟩ and smallest for ⟨100⟩, consistent with the magnetic anisotropy favoring the propagation of the helical order at zero field along ⟨100⟩ [27,29,30].

Typical integrated rocking scans are shown in Fig. 3. Magnetic rocking widths were small in all magnetic phases. An exception was the plane perpendicular to the applied field in the A phase, where the precise intensity distribution was also sensitive to the field and temperature history. Future studies have to establish whether this is due to demagnetizing fields related to the shape of our sample as observed in MnSi [31]. For $B = 0$, the intensity pattern consists of well-defined spots at $k \sim (0.0102 \pm 0.0008)$ Å^{-1} along all three ⟨100⟩ axes, characteristic of a modulation with a long wavelength $\lambda_h \approx 616 \pm 45$ Å. This is shown in Figs. 3(a) and 3(b), which display the intensity patterns for neutrons parallel ⟨100⟩ and ⟨110⟩ respectively. Preliminary tests with polarized neutrons suggest a homochiral helical modulation. The weak

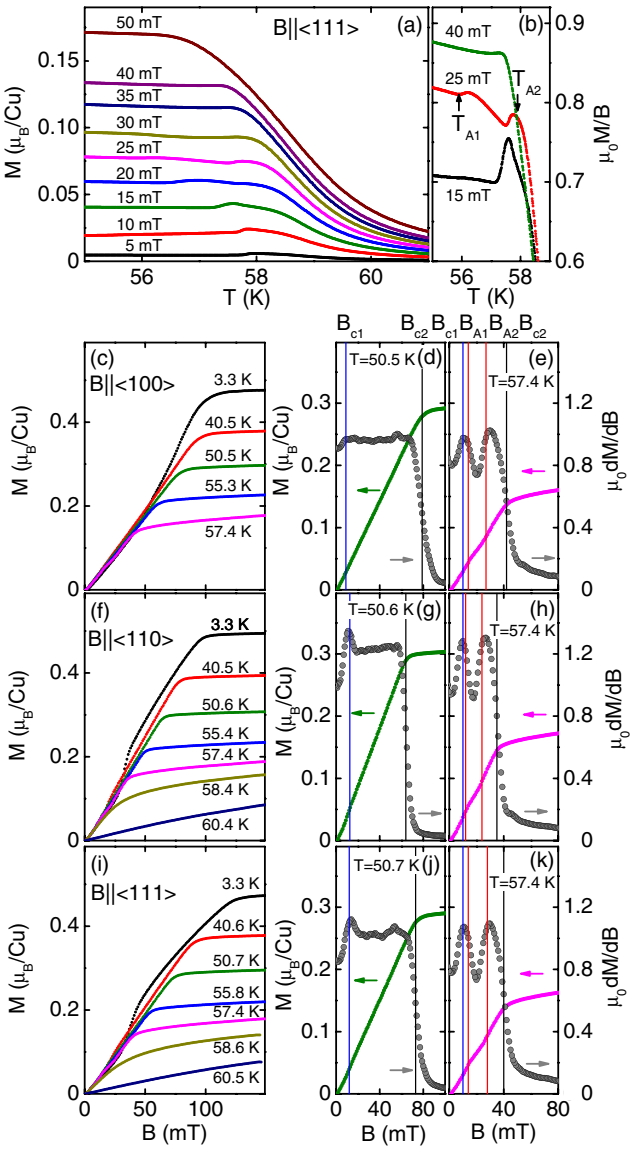

FIG. 1 (color online). Magnetization of single crystal Cu_2OSeO_3 for various crystallographic directions. (a) Temperature dependence of the magnetization in the vicinity of T_c. (b) Ratio $\mu_0 M/B$ versus temperature revealing the features characteristic of the transition to the A phase. Panels (c) through (j): Magnetization as a function of field at various temperatures. Panels on the right-hand side show typical data just below T_c, where a clear minimum in $\mu_0 dM/dB$, calculated from the magnetization, is observed in the A phase.

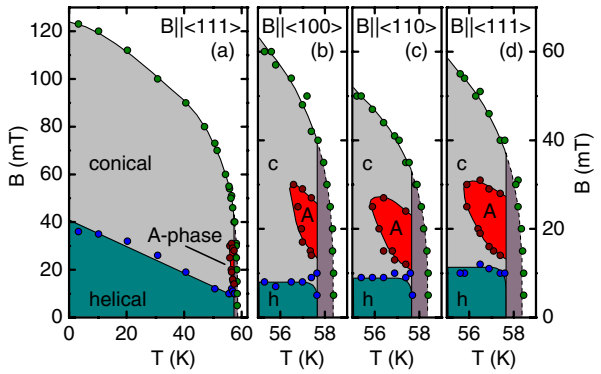

FIG. 2 (color online). Magnetic phase diagram of Cu_2OSeO_3 as a function of applied magnetic field for various orientations inferred from the magnetization. (a) Overview for field parallel $\langle 111 \rangle$. Panels (b) through (d): Phase diagram in the vicinity of T_c for various orientations. Differences as a function of field are mostly due to demagnetizing effects; the brown shading indicates the regime of nearly critical spin fluctuations.

additional spots along the $\langle 110 \rangle$ axes [Fig. 3(a)] are characteristic of double scattering. By analogy with the binary $P2_13$ systems, the scattering pattern at $B = 0$ is characteristic of a multidomain single-$\vec{k}$ helimagnetic state, where spots along each $\langle 100 \rangle$ axes correspond to different domain populations. In contrast, in MnSi, the helical modulation is along $\langle 111 \rangle$. This implies a change of sign of the leading order magnetic anisotropy in Cu_2OSeO_3 [20,21,29,30] but contrasts distinctly the $\langle 110 \rangle$ propagation direction in thin samples [17].

In the range $B_{c1} < B < B_{c2}$, the zero-field pattern [Figs. 3(a) and 3(b)] collapses into two spots parallel to the field, as shown for $B = 58$ mT and $T = 5$ K in Fig. 3(c). Accordingly, the modulation is parallel to B and, in analogy with the binary $P2_13$ compounds, characteristic of a spin-flop phase also known as conical phase.

In the A phase, finally, the intensity pattern consists essentially of a ring of six spots perpendicular to the field, regardless of the orientation of the sample with respect to the field [Figs. 3(d) through 3(h)]. We begin with panel (d) which demonstrates that the pattern for field perpendicular to the neutron beam is also perpendicular to the field. Further, Figs. 3(e) through 3(h) show the six-fold pattern for field parallel to the neutron beam. The six-fold pattern in the plane perpendicular to the field is thereby roughly aligned along $\langle 100 \rangle$, consistent with very weak magnetic anisotropy terms that are sixth order in spin-orbit coupling and small demagnetizing fields (see, e.g., [20,21]).

As demonstrated for the binary $P2_13$ compounds, the six-fold pattern arises from a triple-$\vec{k}$ state, with $\sum_i \vec{k}_i = \vec{0}$, coupled to the uniform magnetization and stabilized by thermal Gaussian fluctuations (a single-$\vec{k}$ modulation perpendicular to the applied field is energetically unfavorable [20]). The topology of the triple-$\vec{k}$ state is that of a

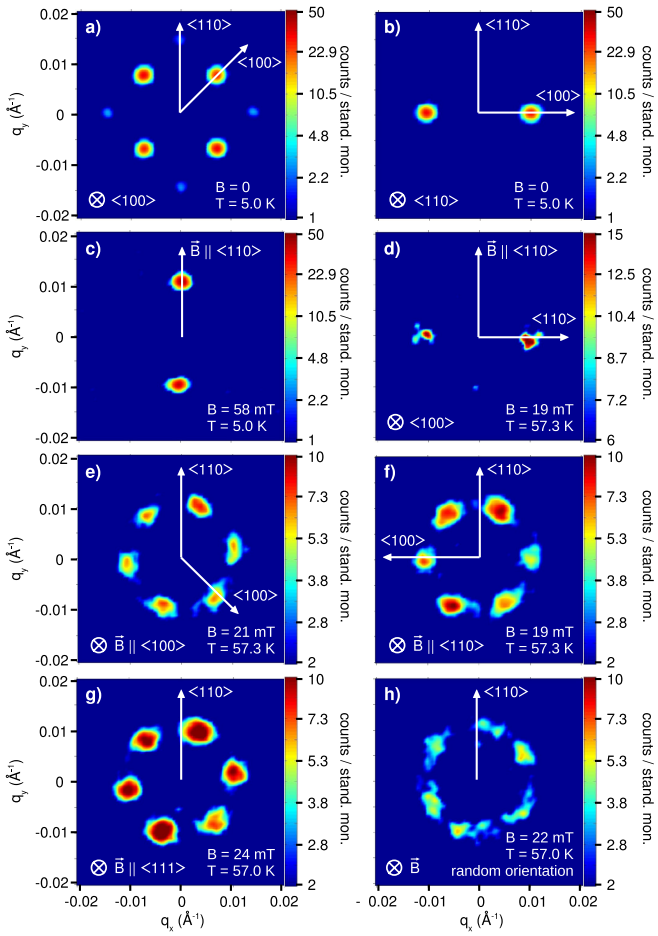

FIG. 3 (color online). Typical integrated small-angle neutron scattering rocking scans in Cu_2OSeO_3. Data are shown as counts per standard monitor (stand. mon.). (a) Zero-field scattering pattern along $\langle 100 \rangle$, characteristic of helimagnetic order along $\langle 100 \rangle$. (b) Zero-field scattering pattern along $\langle 110 \rangle$, characteristic of helimagnetic order along $\langle 100 \rangle$. (c) Typical scattering pattern in the field range $B_{c1} < B < B_{c2}$ for $T \ll T_c$. (d) Scattering pattern in the A phase for magnetic field perpendicular to the neutron beam. Panels (e) through (h): Typical scattering pattern in the A phase for magnetic field parallel to the neutron beam for various orientations.

skyrmion lattice, i.e., the winding number is -1 per magnetic unit cell. This has been confirmed experimentally in MnSi by means of Renninger scans in SANS [31] and the topological Hall signal [32]. We therefore interpret the A phase in Cu_2OSeO_3 as a skyrmion lattice consistent with Refs. [16,17], where microscopic proof for the correct winding number is beyond the scope of our study.

We confirmed that the temperature and field range of the SANS patterns shown in Fig. 3 correspond with Fig. 2. Typical temperature and field dependencies of peak intensities, shown in Fig. 4, provide qualitative information (note that absolute intensities may therefore not be compared easily between the different phases in this figure). We find: (i) the helical order at $B = 0$ is characteristic of a second order phase transition at T_c [Fig. 4(a)]; (ii) the

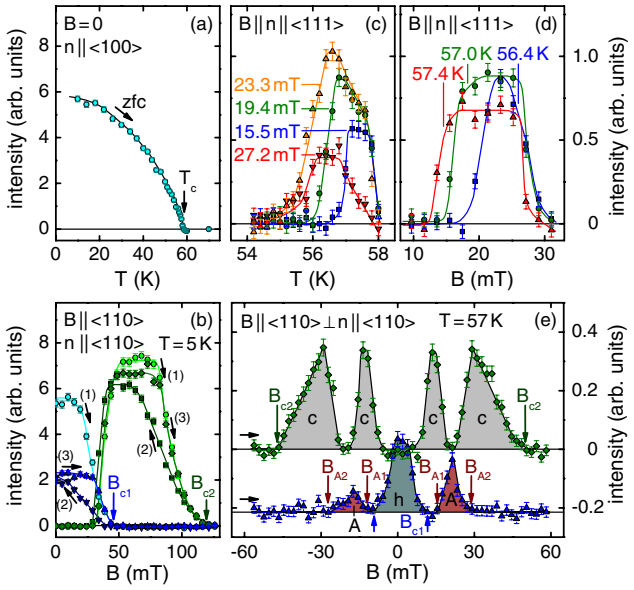

FIG. 4 (color online). Typical temperature and magnetic field dependencies of peak intensities recorded in SANS (see text for details). (a) Temperature dependence of the helical order, cf., Fig. 3(a). (b) Field dependence of the helical and conical state, where triangles correspond the helical state, cf., Fig. 3(b), and squares to the conical state, cf., Fig. 3(c). Labels (1), (2), and (3) mark the sequence in which sweeps were recorded; arrows show the sweep direction. Panels (c) and (d): Temperature and field dependence in the A phase, cf., Fig 3(g). (e) Field dependence in the temperature range of the A phase; helical order (triangles, marked h), conical order (squares, marked c) and A phase (triangles, marked A), cf., Figs. 3(b)–3(d).

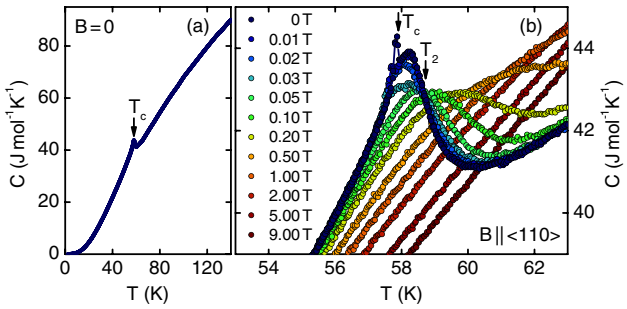

FIG. 5 (color online). Specific heat, C, of Cu_2OSeO_3. With increasing temperature the helimagnetic transition is characterized by peak at T_c followed by a hump with a point of inflection at T_2. The lack of field dependence at T_2 is known as Vollhardt invariance. The B and T dependence of C is characteristic of nearly critical helimagnetic spin fluctuations.

transition from the helical to the conical state is at B_{c1} and the suppression of the conical state at B_{c2} [cf., Fig. 4(b)]; and (iii) in the A phase the signal of the conical phase vanishes completely in a narrow range [Fig. 4(e)]. It seems likely that the regime of the coexistence of the conical phase and the A phase is determined by demagnetizing fields as recently observed in MnSi [27].

At the accuracy of our SANS data, the transition at T_c is second order [cf., Fig. 4(a)]. However, the specific heat, C, shown in Figs. 5(a) and 5(b), reveals that the transition consists of a narrow peak at T_c, characteristic of the latent heat of a first order transition, and a broad hump with a point of inflection at T_2. Under magnetic fields, the peak and hump are suppressed with a shift of entropy toward high temperatures, while the point of inflection at T_2 does not change for $B \lesssim B_{c2}$, characteristic of a Vollhardt invariance [33]. For the case of MnSi, the same behavior is due to a fluctuation-induced first-order transition, where the helimagnetic character of the fluctuations becomes dominant for $T < T_2$, [28,34–37]. In turn, this suggests that the enhanced MDR arises from spin currents associated with the helimagnetic character of the spin fluctuations. As the MDR is quantitatively rather small, a full account connecting the magnetic with the dielectric susceptibility poses a challenge for future studies. Interestingly, the enhanced MDR in $Dy_2Ti_2O_7$ [9] might originate in similar spin currents associated with chiral spin excitations, where, however, the chiral character originates in geometric frustration rather than DM interactions.

The consistency of the magnetic properties of bulk samples of Cu_2OSeO_3 with the binary $P2_13$ compounds is surprising as the unit cell of Cu_2OSeO_3 contains 28, instead of 8, atoms. Thus, bulk samples of Cu_2OSeO_3 represent the first example of helimagnetic order in a structural sibling of the B20 compounds that is nonbinary, an oxide, a compound with a nonferromagnetic leading-order exchange interaction, and an insulator. Interestingly, the skyrmion lattice phase extends, thereby, over a similar temperature range, regardless of whether the material is metallic, semiconducting, or insulating. This provides an important test of different microscopic mechanisms proposed to stabilize the skyrmion lattice, e.g., thermal Gaussian fluctuations [20] or a reduced stiffness of the magnetization modulus [38,39], where the latter is expected to differ strongly between metals and insulators [38]. Further, the helimagnetism resolves the open questions concerning the magnetization of Cu_2OSeO_3, explaining enhancements of the MDR even for nonmultiferroic systems such as $Dy_2Ti_2O_7$. Being an insulator, the skyrmion lattice in Cu_2OSeO_3 thereby promises an emergent electrodynamics akin to that observed in its binary siblings [24,25], where electric fields may now be used to manipulate the skyrmions.

We wish to thank P. Böni, M. Garst, R. Georgii, M. Halder, H. Kolb, S. Mayr, J. Peters, W. Petry, and A. Rosch for support and stimulating discussions. Financial support through DFG TRR80, FOR960, the NTH School "Contacts in Nanosystems," and ERC AdG (291079) TOPFIT are gratefully acknowledged. T. A., A. C., M. W., A. B., and G. B. acknowledge support through the TUM Graduate School.

*christian.pfleiderer@frm2.tum.de

[1] W. Erenstein, N. D. Mathur, and J. F. Scott, Nature (London) **442**, 759 (2006).
[2] M. Fiebig, J. Phys. D **38**, R123 (2005).
[3] N. Spaldin and M. Fiebig, Science **309**, 391 (2005).
[4] S. Cheong and M. Mostovoy, Nature Mater. **6**, 13 (2007).
[5] J.-W. G. Bos, C. V. Colin, and T. T. M. Palstra, Phys. Rev. B **78**, 094416 (2008).
[6] V. P. Gnezdilov, K. V. Lamonova, Y. G. Pashkevich, P. Lemmens, H. Berger, F. Bussy, and S. L. Gnatchenko, Low Temp. Phys. **36**, 550 (2010).
[7] M. I. Kobets, K. G. Dergachev, E. N. Khatsko, A. I. Rykova, P. Lemmens, D. Wulferding, and H. Berger, Low Temp. Phys. **36**, 176 (2010).
[8] K. H. Miller, X. S. Xu, H. Berger, E. S. Knowles, D. J. Arenas, M. W. Meisel, and D. B. Tanner, Phys. Rev. B **82**, 144107 (2010).
[9] M. Saito, R. Higashinaka, and Y. Maeno, Phys. Rev. B **72**, 144422 (2005).
[10] P. G. Meunier and M. Bertaud, J. Appl. Crystallogr. **9**, 364 (1976).
[11] H. Effenberger and F. Pertlik, Monatshefte für Chemie **117**, 887 (1986).
[12] K. Kohn, J. Phys. Soc. Jpn. **42**, 2065 (1977).
[13] M. Belesi, I. Rousochatzakis, H. C. Wu, H. Berger, I. V. Shvets, F. Mila, and J. P. Ansermet, Phys. Rev. B **82**, 094422 (2010).
[14] C. L. Huang, K. F. Tseng, C. C. Chou, S. Mukherjee, J. L. Her, Y. H. Matsuda, K. Kindo, H. Berger, and H. D. Yang, Phys. Rev. B **83**, 052402 (2011).
[15] M. Belesi, T. Philipp, I. Rousochatzakis, H. C. Wu, H. Berger, S. Granvlle, I. V. Shvets, and J. P. Ansermet, J. Phys. Conf. Ser. **303**, 012069 (2011).
[16] Our study was inspired by a preliminary report of Lorentz force microscopy in thin Cu_2OSeO_3 samples by S. Seki *et al.*, Report No. FIRST-QS2C, FIRST-QS2C workshop on Emergent Phenomena of Correlated Materials, Okinawa, 2011 (unpublished).
[17] S. Seki, X. Z. Yu, S. Ishiwata, and Y. Tokura, Science **336**, 198 (2012).
[18] Determination of the correct magnetoelectric coupling requires measurements of the full coupling tensor, which is beyond the scope of our study.
[19] L. D. Landau and E. M. Lifshitz, *Course of Theoretical Physics* (Pergamon Press, New York, 1980), Vol. 8.
[20] S. Mühlbauer, B. Binz, F. Jonietz, C. Pfleiderer, A. Rosch, A. Neubauer, R. Georgii, and P. Böni, Science **323**, 915 (2009).
[21] W. Münzer, A. Neubauer, T. Adams, S. Mühlbauer, C. Franz, F. Jonietz, R. Georgii, P. Böni, B. Pedersen, M. Schmidt *et al.*, Phys. Rev. B **81**, 041203(R) (2010).
[22] X. Z. Yu, Y. Onose, N. Kanazawa, J. H. Park, J. H. Han, Y. Matsui, N. Nagaosa, and Y. Tokura, Nature (London) **465**, 901 (2010).
[23] X. Z. Yu, N. Kanazawa, Y. Onose, K. Kimoto, W. Z. Zhang, Y. Matsui, and Y. Tokura, Nature Mater. **10**, 106 (2011), published online 05 December 2010.
[24] T. Schulz, R. Ritz, A. Bauer, M. Halder, M. Wagner, C. Franz, C. Pfleiderer, K. Everschor, M. Garst, and A. Rosch, Nature Phys. **8**, 301 (2012).
[25] F. Jonietz, S. Mühlbauer, C. Pfleiderer, A. Neubauer, W. Münzer, A. Bauer, T. Adams, R. Georgii, P. Böni, R. A. Duine *et al.*, Science **330**, 1648 (2010).
[26] See Supplemental Material at http://link.aps.org/supplemental/10.1103/PhysRevLett.108.237204 for an account of the method of crystal growth, tests of sample quality, the set-up used for neutron scattering as well as other experimental aspects.
[27] A. Bauer, C. Pfleiderer, Magnetic Phase Diagram of MnSi Inferred from Magnetisation and AC Susceptibility Measurements, Phys. Rev. B (to be published).
[28] A. Bauer, A. Neubauer, C. Franz, W. Münzer, M. Garst, and C. Pfleiderer, Phys. Rev. B **82**, 064404 (2010).
[29] P. Bak and M. H. Jensen, J. Phys. C **13**, L881 (1980).
[30] O. Nakanishi, A. Yanase, A. Hasegawa, and M. Kataoka, Solid State Commun. **35**, 995 (1980).
[31] T. Adams, S. Mühlbauer, C. Pfleiderer, F. Jonietz, A. Bauer, A. Neubauer, R. Georgii, P. Böni, U. Keiderling, K. Everschor *et al.*, Phys. Rev. Lett. **107**, 217206 (2011).
[32] A. Neubauer, C. Pfleiderer, B. Binz, A. Rosch, R. Ritz, P. G. Niklowitz, and P. Böni, Phys. Rev. Lett. **102**, 186602 (2009).
[33] D. Vollhardt, Phys. Rev. Lett. **78**, 1307 (1997).
[34] S. V. Grigoriev, S. V. Maleyev, E. V. Moskvin, V. A. Dyadkin, P. Fouquet, and H. Eckerlebe, Phys. Rev. B **81**, 144413 (2010).
[35] M. Janoschek, M. Garst, A. Bauer, P. Krautscheid, R. Georgii, P. Böni, and C. Pfleiderer, arXiv:1205.4780.
[36] S. M. Stishov, A. E. Petrova, S. Khasanov, G. K. Panova, A. A. Shikov, J. C. Lashley, D. Wu, and T. A. Lograsso, Phys. Rev. B **76**, 052405 (2007).
[37] A. Hamann, D. Lamago, T. Wolf, H. v. Löhneysen, and D. Reznik, Phys. Rev. Lett. **107**, 037207 (2011).
[38] U. K. Rößler, A. N. Bogdanov, and C. Pfleiderer, Nature (London) **442**, 797 (2006).
[39] A. B. Butenko, A. A. Leonov, U. K. Rößler, and A. N. Bogdanov, Phys. Rev. B **82**, 052403 (2010).